The Journal of Immunology

Structurally Distinct Membrane Nanotubes between Human Macrophages Support Long-Distance Vesicular Traffic or Surfing of Bacteria

Björn Önfelt, Shlomo Nedvetzki, Richard K. P. Benninger, Marco A. Purbhoo, Stefanie Sowinski, Alistair N. Hume, Miguel C. Seabra, Mark A. A. Neil, Paul M. W. French and Daniel M. Davis

J Immunol 2006; 177:8476-8483; ;
doi: 10.4049/jimmunol.177.12.8476
http://www.jimmunol.org/content/177/12/8476

The Journal of Immunology is published twice each month by
The American Association of Immunologists, Inc.,
1451 Rockville Pike, Suite 650, Rockville, MD 20852

Print ISSN: 0022-1767 Online ISSN: 1550-6606.

Structurally Distinct Membrane Nanotubes between Human Macrophages Support Long-Distance Vesicular Traffic or Surfing of Bacteria[1]

Björn Önfelt,[2]* Shlomo Nedvetzki,* Richard K. P. Benninger,† Marco A. Purbhoo,* Stefanie Sowinski,* Alistair N. Hume,‡ Miguel C. Seabra,‡ Mark A. A. Neil,† Paul M. W. French,† and Daniel M. Davis[3]*

We report that two classes of membrane nanotubes between human monocyte-derived macrophages can be distinguished by their cytoskeletal structure and their functional properties. Thin membrane nanotubes contained only F-actin, whereas thicker nanotubes, i.e., those > ~0.7 μm in diameter, contained both F-actin and microtubules. Bacteria could be trapped and surf along thin, but not thick, membrane nanotubes toward connected macrophage cell bodies. Once at the cell body, bacteria could then be phagocytosed. The movement of bacteria is aided by a constitutive flow of the nanotube surface because streptavidin-coated beads were similarly able to traffic along nanotubes between surface-biotinylated macrophages. Mitochondria and intracellular vesicles, including late endosomes and lysosomes, could be detected within thick, but not thin, membrane nanotubes. Analysis from kymographs demonstrated that vesicles moved in a stepwise, bidirectional manner at ~1 μm/s, consistent with their traffic being mediated by the microtubules found only in thick nanotubes. Vesicular traffic in thick nanotubes and surfing of beads along thin nanotubes were both stopped upon the addition of azide, demonstrating that both processes require ATP. However, microtubule destabilizing agents colchicine or nocodazole abrogated vesicular transport but not the flow of the nanotube surface, confirming that distinct cytoskeletal structures of nanotubes give rise to different functional properties. Thus, membrane nanotubes between macrophages are more complex than unvarying ubiquitous membrane tethers and facilitate several means for distal interactions between immune cells. ***The Journal of Immunology,*** **2006, 177: 8476–8483.**

The study by Rustom et al. (1) reported that rat neuronal PC12 cells, and other cells, could be connected by tunneling nanotubes. These nanotubes were shown to mediate transfer of lipid organelles between cells by actin-dependent mechanisms. Membrane-bound proteins were also seen to diffuse between cells, suggesting a seamless transition of the plasma membranes of the two cells. However, there was some selection in what could transfer between cells because small cytoplasmic molecules, such as calcein, could not diffuse along nanotubes. Nanotubular structures were also reported to connect a range of immune cells, such as B cells, T cells, NK cells, and monocyte-derived macrophages (2, 3). Membrane nanotubes were observed, for example, between NK cells and B cells upon disassembly of immunological synapses (3). Membrane nanotubes thus represent one mechanism that could facilitate the commonly observed intercellular exchange of cell surface proteins and lipids (2, 4–12).

Most recently, Watkins and Salter (13) reported that myeloid cells can transmit calcium signals through nanotubes. After receiving a nanotube-mediated calcium signal, dendritic cells were observed to spread membrane veils toward the origin of the signal (13), similar to the response observed toward Ags (14). Thus, signals transmitted via membrane nanotubes between myeloid cells could augment immune responses at sites distal to the triggering Ag.

In this study, we demonstrate an unexpected heterogeneity in the cytoskeletal structure of membrane nanotubes connecting human macrophages. Importantly, this heterogeneity in structure underpins distinct functional properties of membrane nanotubes: thick nanotubes traffic intracellular vesicles along microtubules, whereas thin nanotubes facilitate transport of bacteria along their surface toward macrophage cell bodies. The latter is reminiscent of recent observations that virus particles can move along the surface of filopodia, a process recently termed surfing (15).

Materials and Methods

Generation of macrophages

Human monocyte-derived macrophages were isolated and cultured as previously described (16). Briefly, buffy coat PBMCs (National Blood Transfusion Service, London, U.K.) were isolated by density gradient centrifugation (Ficoll-Paque Plus; Amersham Biosciences). The serum was collected, heat-inactivated for 30 min at 56°C, and filtered. PBMCs were incubated for 2 h in plastic plates previously coated overnight with 2% gelatin (Sigma-Aldrich). After 2 h the flask was washed intensively to remove the nonadherent cells. After 24 h of incubation in serum-free medium (X-Vivo 10; BioWhittaker) with 1% autologous serum, monocytes were washed with cold PBS, and CD14 expression was assessed by flow cytometry (CellQuest; BD Biosciences), which showed 98% of the cells CD14-positive. Monocytes were then cultured in X-Vivo medium with 1%

*Division of Cell and Molecular Biology, †Department of Physics, and ‡Molecular and Cellular Medicine, National Heart and Lung Institute, Imperial College London, South Kensington Campus, London SW7 2AZ, United Kingdom

Received for publication April 12, 2006. Accepted for publication October 6, 2006.

The costs of publication of this article were defrayed in part by the payment of page charges. This article must therefore be hereby marked *advertisement* in accordance with 18 U.S.C. Section 1734 solely to indicate this fact.

[1] This work was supported by a fellowship from the Wenner-Gren Foundations (to B.Ö.), the Medical Research Council (U.K.), the Wellcome Trust, the Biotechnology and Biological Sciences Research Council, and the U.K. Department of Trade and Industry (Beacon Project). D.M.D. is a recipient of a Lister Institute Research Prize.

[2] Current address: Microbiology and Tumor Biology Center and Strategic Research Center for Studies of Integrated Recognition in the Immune System, Karolinska Institute, Stockholm, Sweden.

[3] Address correspondence and reprint requests to Dr. Daniel M. Davis, Division of Cell and Molecular Biology, Sir Alexander Fleming Building, Imperial College London, South Kensington Campus, London SW7 2AZ, U.K. E-mail address: d.davis@imperial.ac.uk

0022-1767/06/$02.00

autologous serum for 8–12 days in eight-well chamber slides (LabTek; Nunc), at a density of ~750 cells per mm^2, replacing the medium every 3 days. For the majority of the experiments, uncoated glass substrates were used, but to test the influence of different culturing conditions and substrates on tube formation, chamber slides were coated overnight with 100 ng/ml fibronectin (Sigma-Aldrich) or 100 ng/ml collagen (Sigma-Aldrich) before seeding, or cells were grown in a presence of 50 ng/ml recombinant human M-CSF (PeproTech). Thereafter, the relative number of thick and thin nanotubes was assessed by counting.

Transfection of macrophages

Plasmid pEGFPN2-EB1, which allows expression of a fusion protein of EB1 C terminus tagged with enhanced GFP, was created by PCR amplification of the full murine EB1 coding sequence from IMAGE clone 5057090 using primers EB1 sense 5′-CCGGAATTCAGATCTATGGA CATGCTC TTCCCTG and EB1 antisense 5′-GCCGCTCGAGTTAATA CTCTTCTTGTTCCTC. The PCR product was then subcloned into the pEGFPN2 vector (Clontech Laboratories) using restriction endonucleases *Eco*R1 and *Xho*I for insert DNA and *Eco*R1 and *Sal*I for vector DNA. For transfection, day 6–10 primary macrophage cultures were detached by 1 h incubation in trypsin/EDTA (Sigma-Aldrich) at 37°C, followed by gentle scraping. Macrophages were pelleted and 1–2 $\times$ 10^6 cells transfected with 0.5 μg of pEGFPN2-EB1 by electroporation (human macrophage electroporation kit using program Y-10; Amaxa). Cells were resuspended in 1 ml of macrophage medium, plated into eight-well chamber slides, and imaged 24–48 h after transfection.

Bacteria and beads

Mycobacterium bovis bacillus Calmette-Guérin (BCG)[4] expressing GFP, a gift from D. Young, Imperial College (London, U.K.), was cultured as previously described (17). For experiments, BCG-GFP were washed and resuspended in warm medium and added to the imaging chamber to an average multiplicity of infection of 12. When appropriate, macrophages were surface-biotinylated by incubation with 0.5 mg/ml Sulfo-NHS-LC-biotin (sulfosuccinimidyl-6-(biotinamido) hexanoate, EZ-Link; Pierce)/PBS for 15 min at 37°C, quenched with warm PBS complemented with 50 mM NH_4Cl, washed in warm PBS and incubated with streptavidin-coated fluorescent beads with a mean diameter of 1.6 μm (Bangs Laboratories). Cells were imaged ~0–3 h after addition of bacteria or beads.

Live cell reagents and drugs

To investigate the transport of lipid vesicles, macrophages were stained with DiD (1,1′-dioctadecyl-3,3,3′,3′-tetramethylindodicarbocyanine perchlorate; Molecular Probes) according to supplier's instructions and left to rest overnight before imaging. Acidic lysosomes or mitochondria were visualized by staining with LysoTracker Red DND-99 or MitoTracker Deep Red 633 according to supplier's instructions (Molecular Probes). To investigate whether transport along nanotubes was dependent on ATP and the cytoskeleton, 100 mM azide (Sigma-Aldrich), 10 μM colchicine (Sigma-Aldrich), 15 μM nocodazole (Sigma-Aldrich), 10 μM cytochalasin D (Sigma-Aldrich), or 0.3–10 μM latrunculin B was added to the imaging chamber.

Fixation and immunostaining

For immunostaining, macrophages were fixed with 0.1% glutaraldehyde/4% paraformaldehyde in PBS for 1 min at room temperature followed by further fixation with either Cytofix/Cytoperm (BD Biosciences) for 5 min at 37°C or 4% paraformaldehyde for 15 min at room temperature. For fluorescence staining of F-actin, cells were incubated with phalloidin-Alexa Fluor 633 or phalloidin-Alexa Fluor 635 (Molecular Probes). Abs for immunofluorescence were mouse anti-α-tubulin mAb (clone DM1A; Sigma-Aldrich), mouse anti-lysosome-associated membrane protein (LAMP)-1 mAb (clone H4A3), mouse IgG1 isotype control mAb (both from BD Biosciences), and Alexa Fluor 488-labeled goat anti-mouse IgG (Molecular Probes). All incubations were performed for 45 min at 4°C in 3% BSA, 5% horse serum in buffer containing detergents (Perm/Wash; BD Biosciences).

Microscopy

All live cell imaging was performed by confocal microscopy (TCS SP2 RS; Leica Microsystems), equipped with an environmental chamber (Solent Scientific) kept at 37°C/5% CO_2. When necessary, the pinhole was opened to capture more fluorescence at the cost of obtaining thicker optical sections. Brightness and contrast were changed in some images, only to increase visibility of nanotubular connections. Confocal stacks were reconstructed for three-dimensional visualization of cells (Volocity; Improvision).

Image analysis

Kymographs were created using routines developed in-house (LabView; National Instruments and MATLAB; The MathWorks). Briefly, a bounding box was drawn over the length and width of the nanotube. For each frame of the time-lapse sequence, the bounding box data was summed perpendicular to the nanotube to give an intensity profile down the length of the nanotube, and profiles stitched together to create a time-position image (i.e., a kymograph). Kymographs were then normalized according to both position and time to reduce the effect of permanent bright features such as at the nanotube ends, and the effect of photobleaching. Kymographs were finally smoothed using a 3 $\times$ 3 filter. Brightness and contrast were changed in some kymographs to increase visibility. Speeds and distances were calculated from the coordinates of trajectories. Limits in temporal and spatial resolution made it difficult to identify vesicle paths shorter than ~1 μm.

Results

Distinct types of long-distance intercellular membrane tethers connect human macrophages

Human monocyte-derived macrophages were seen to be connected by multiple membrane tethers or nanotubes. Most nanotubes were raised above the coverslip and connected apical parts of the cells. Importantly, these nanotubes were not vestiges of cytokinesis because human monocyte-derived macrophages do not divide under the culturing conditions used (data not shown). Staining for α-tubulin and F-actin revealed that some nanotubes contained microtubules and F-actin, whereas other nanotubes contained only F-actin (Fig. 1, *A* and *B*). To test whether microtubules could grow seamlessly from within a cell body into a nanotube, macrophages transfected to express EB1-GFP, which is associated with plus ends of growing microtubules (18), were imaged by time-lapse microscopy. Bright EB1-GFP "rockets" were observed to stop and abruptly disappear at the base of some nanotubes (Fig. 1*C* and supplemental video 1),[5] although they were readily observed to move inside other nanotubes (Fig. 1*D* and supplemental video 2).[5] In this model, EB1-GFP was observed to move freely into the nanotube at one end but was not observed to enter the cell body at the other end, in which the nanotube instead formed a bulbous tip (Fig. 1*D*). Surprisingly, considering its polarized association with microtubules, EB1-GFP rockets were observed to travel in both directions inside this membrane nanotube. Most importantly, these data further established that microtubule growth only occurs within a subset of nanotubes that connect macrophages.

Some images of fixed cells stained with anti-α-tubulin mAb showed no apparent junction separating the microtubule networks originating from different cell bodies connected by a nanotube (Fig. 1, *E–G*). This finding suggests that at least some nanotubular connections could be open at both ends, thereby joining cell bodies together. Interestingly, albeit rarely, nanotubes were seen branched such that three cells could be connected together simultaneously (Fig. 1*H*).

Brightfield images clearly showed heterogeneity in the morphology of membrane nanotubes, most noticeably seen in nanotubes having different diameters. Importantly, nanotubes containing both F-actin and microtubules were thicker, i.e., $\geq$0.7 μm, than those that only contained F-actin (Fig. 1*I*). Both the total number of nanotubes and the ratio of thin to thick connections (~2:1) were very similar whether cells were grown on glass, fibronectin or

[4] Abbreviations used in this paper: BCG, bacillus Calmette-Guérin; LAMP, lysosome-associated membrane protein.

[5] The online version of this article contains supplemental material.

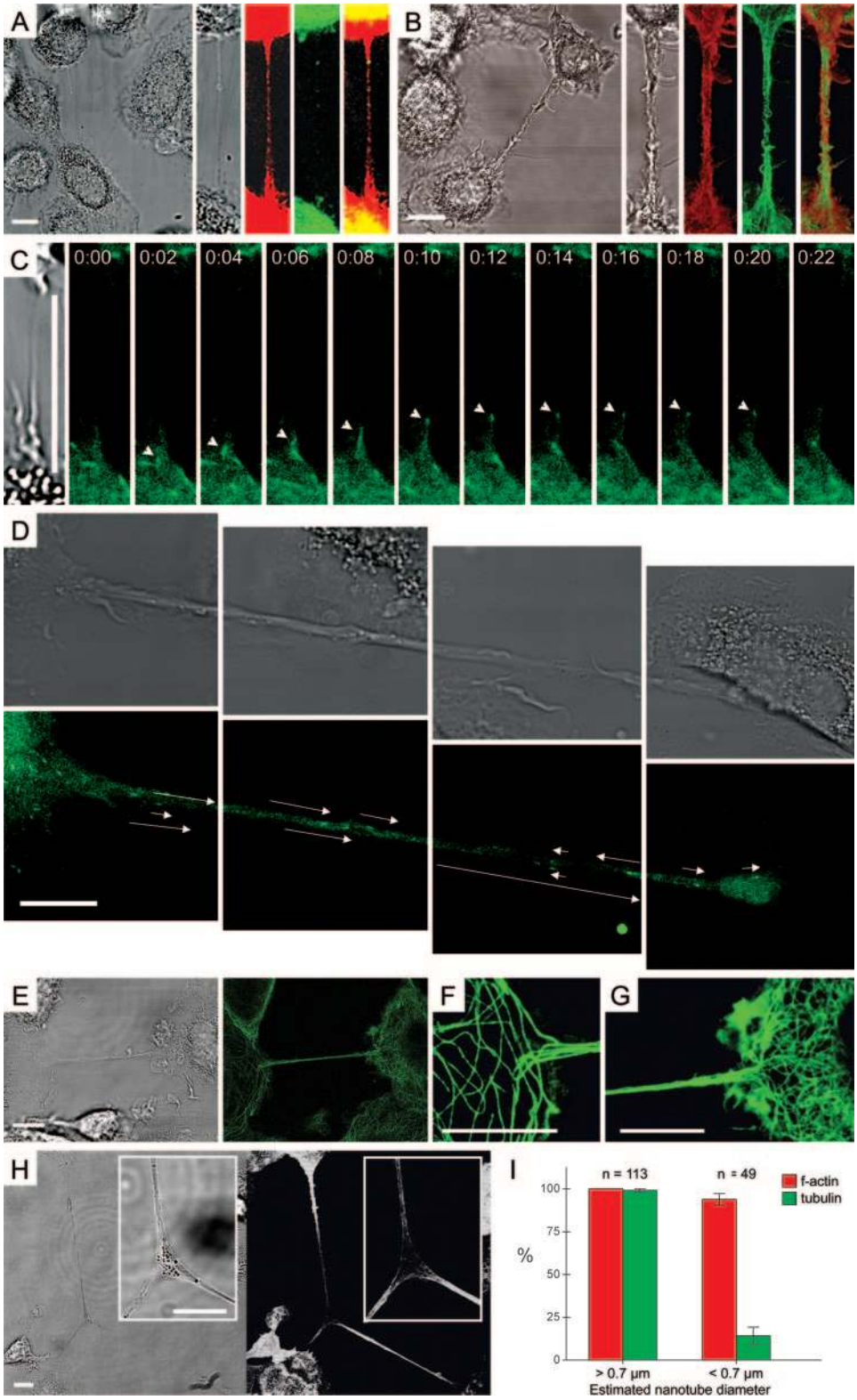

FIGURE 1. Heterogeneity in the cytoskeletal structure of membrane nanotubes. *A*, Some membrane nanotubes between macrophages contained F-actin (stained by phalloidin; red) but not microtubules (stained with mAb against α-tubulin; green). *B*, Other nanotubes contained both F-actin and microtubules. *C–D*, EB1-GFP, which binds to the leading end of growing microtubules, can only enter some nanotubes. *C*, Time-lapse sequence shows a rocket of high density EB1-GFP (arrowhead), representing a growing microtubule, traveling in the cell body to the base of a thin membrane nanotube where it stops. In the last time frame, the EB1-GFP cluster disappeared, consistent with discontinued growth of the microtubule. *D*, A mosaic made up from four images at different positions along a membrane nanotube. Time-lapse microscopy at each section of the nanotube revealed several EB1-GFP rockets inside. Arrows mark the direction and distance traveled of rockets seen in the image shown. *E–G*, Staining of α-tubulin (green) suggests no intercellular junction in the microtubule network between the two connected cells. Enlarged views are shown for left (*F*) and right (*G*) contacts between the nanotube and two cell bodies shown in *E*. *H*, Three macrophages networked by a branched membrane nanotube. Cells were stained for F-actin (phalloidin, white). Enlarged view (*inset*) of the junction are shown. All fluorescence images, other than those in *C–E*, are reconstructed from several optical slices. Scale bars, 20 μm. *I*, Nanotubes were counted as either thick or thin by their diameter being estimated to be above or below 0.7 μm, respectively. Thick nanotubes commonly contained both microtubules and F-actin, whereas thin nanotubes usually only contained F-actin. Error bars represent SD of binomial distribution.

collagen, or in presence of M-CSF (data not shown). Thus, membrane nanotubes connecting macrophages can form under various culture conditions and are heterogeneous in their cytoskeletal composition.

Membrane nanotubes can form as macrophages separate after contact

Live cell imaging extending over several hours showed that membrane nanotubes could be formed as migrating macrophages separated after contact (Fig. 2*A* and supplemental video 3).[5] Thick nanotubular connections could remain stable for several hours, but we also observed their disassembly through apparent retraction of part of the nanotube, leaving a thin nanotube (Fig. 2, *B* and *C*). Such retraction could start either from the base of the nanotube close to one of the connecting cell bodies (Fig. 2*B*), or from a point in the middle of the nanotube (Fig. 2*C*). It has been shown previously that nanotubular connections could create large and complex networks of myeloid cell bodies (13, 19). Thus, membrane nanotubes can

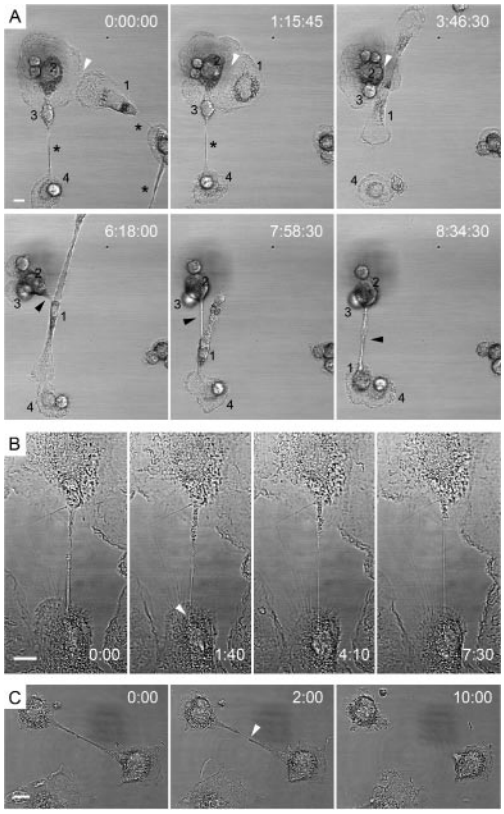

FIGURE 2. Membrane nanotubes can form as migrating cells separate after contact. *A*, Brightfield time-lapse sequence show several macrophages (some labeled 1–4) connected by membrane nanotubes (⋆). Macrophage 1 migrates to form a tight intercellular contact with macrophage 2 (white arrowhead), and then macrophage 1 elongates (t = ~3–7 h), and as the cells separate a membrane nanotube is formed (black arrowheads at $t >$ 6 h). Time format is hours:minutes:second. *B* and *C*, Thin nanotubes can form through retraction of thick nanotubes. Time format is minutes:second. *B*, Time-lapse sequence shows two macrophages connected by a nanotube. At t = 1:40, the nanotube starts to retract from the base at the connection with the lower cell (arrowhead), leaving the cells connected by a thinner nanotube. *C*, Same as in *B*, but the retraction starts from a point in the middle of the tube (arrowhead), again leaving the cells connected by a thinner tube. Scale bar, 20 μm.

form as cells separate after contact and can connect macrophages into large and complex cell networks.

Bacteria surf along thin membrane nanotubes to macrophage cell bodies

Individual *M. bovis* BCG or clusters of several bacteria could bind to the surface of nanotubes between macrophages. Time-lapse imaging showed that bacteria could be transported along thin nanotubes to connected cell bodies (Fig. 3*A* and supplemental videos 4 and 5).[5] After surfing to the end of a nanotube, bacteria could be internalized into the cell body (Fig. 3*B*), within a time consistent with previous observations of phagocytosis of bacteria (20, 21). Thus, bacteria can be trapped and transported along thin membrane nanotubes for phagocytosis at the macrophage cell body. Importantly, bacteria also adhered to the surface of thick nanotubes but surfing toward cell bodies was not observed along these nanotubes (Fig. 3*C*). Thus, bacteria can be trapped and transported along thin but not thick membrane nanotubes for phagocytosis at the macrophage cell body.

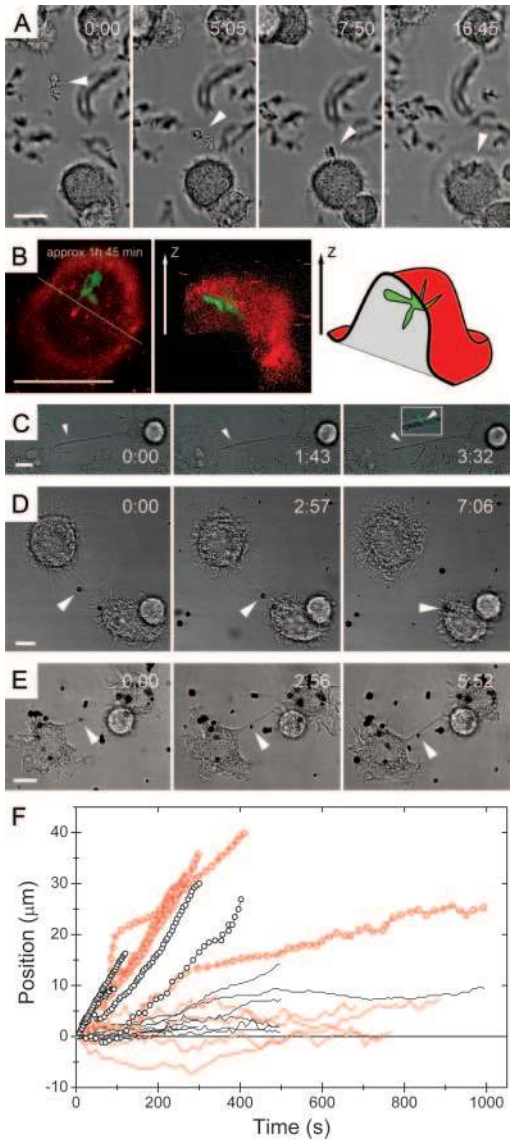

FIGURE 3. Bacteria can surf along membrane nanotubes, aided by constitutive flow of nanotube surface. *A*, Brightfield time-lapse imaging shows *Mycobacterium bovis* BCG bacteria expressing GFP, incubated with human macrophages. A cluster of bacteria (arrowhead) is shown trapped on a membrane nanotube connecting two macrophages. Bacteria were transported along the nanotube to the cell body where they were phagocytosed. *B*, To confirm that the bacteria were indeed internalized, the cell membrane was labeled by addition of DiD directly to the imaging chamber. A reconstructed view (*left*) from the top of the macrophage, the cross-section (*middle*, along the thin white line in the left panel) of the same image stack, and a schematic drawing (*right*) of this cross-section shown to aid visualization of the fluorescence data are presented. Approximately 1 h and 45 min elapsed between the time when the bacteria (*A*) were first observed on the nanotube and the bacteria were phagocytosed (*B*). *C*, Brightfield and fluorescence time-lapse sequences show a bacteria (arrowhead; green) being stationary on the surface of a thick nanotube. An expanded section (*inset*) shows the bacteria on the nanotube (arrowhead). *D* and *E*, Brightfield time-lapse image of streptavidin-coated beads with surface biotinylated macrophages is shown. Time format is minutes:second. *D*, Beads (one marked by arrowhead) bound to the surface of thin membrane nanotubes and were transported to the body of one of the connected macrophages (n = 27). *E*, A bead (arrowhead) remained stationary on the surface of a thicker nanotube (n = 16). Scale bar, 20 μm. *F*, Trajectories of several bacteria (red) and beads (black) along thick (solid lines) and thin (circles) nanotubes. Beads and bacteria surf systematically toward cell bodies along thin but not thick nanotubes.

Constitutive flow aids transport along the surface of thin membrane nanotubes

We next set out to test whether surfing of bacteria along thin nanotubes was aided by a constitutive flow along the nanotube surface. Macrophages were surface-biotinylated and imaged in the presence of streptavidin-coated beads. Indeed, beads were found to surf along thin nanotubes in a manner similar to bacteria (Fig. 3*D* and supplemental video 6).[5] Beads generally traveled unidirectionally toward one of the connected cells with almost constant speed of 0.13 ± 0.02 μm/s. Occasionally, beads moved intermittently in both directions before eventually starting to move steadily toward one of the connected cells (n = 5/27). Thus, there is a constitutive flow along the surface of thin membrane nanotubes, which can carry cargo to macrophage cell bodies.

Similar to bacteria, systematic transport of beads toward cell bodies was not observed along thick nanotubes (Fig. 3*E* and supplemental video 7).[5] Analysis of several bacteria and beads attached to thin and thick tubes showed that the surfing was restricted to thin tubes (Fig. 3*F*). Although bacteria and beads sometimes changed position along the surface of thick nanotubes, this movement did not appear directed or systematic and merely correlated with migration of the connected cells. Thus, thin and thick nanotubes are functionally distinct.

Vesicles and mitochondria are transported within thick membrane nanotubes

Vesicles labeled with the lipophilic dye DiD were readily observed inside thick nanotubes connecting macrophages (Fig. 4, *A* and *B*). For example, two particularly bright DiD-labeled vesicles, or perhaps multivesicular bodies, moved within a nanotube connecting two macrophages, ending up within the cytoplasm of one of the cells (Fig. 4*B* and supplemental video 8).[5] Acidic lysosomes, stained with LysoTracker, were also observed to move within nanotubes (Fig. 4, *C* and *D*). Monoclonal Ab against LAMP-1 showed a clear punctuate staining within thick nanotubes, identifying at least some vesicles in these nanotubes to be late endosomes or lysosomes (Fig. 4*E*). Larger organelles, mitochondria stained by MitoTracker, were also observed inside thick, but not thin, nanotubes between live macrophages (Fig. 4*F*). Thus, a wide variety of intracellular compartments can traffic within thick membrane nanotubes.

Vesicles move stepwise and bidirectionally along microtubules inside thick membrane nanotubes

To analyze the movements of vesicles inside thick membrane nanotubes in more detail, kymographs were plotted. Individual vesicles moved bidirectionally in a stepwise manner inside membrane nanotubes (Fig. 5*A*). Furthermore, vesicles were seen to pass each other, either as they were traveling in the same direction or when moving in opposite directions (data not shown), indicating the presence of several independent "tracks" for vesicular traffic inside nanotubes. Vesicles were sometimes transported the full length of tubular connections and into the cytoplasm of a connected cell body.

By measuring the slope and length of a linear period within vesicle trajectories, the speeds and distances traveled were quantified (Fig. 5*B*). Vesicles inside nanotubes moved with an average speed of 1.01 ± 0.04 μm/s with a maximum speed of ~5 μm/s (Fig. 5*C*). The average distance of a single vesicle "run," i.e., of one continuous vesicle movement before stopping, changing speed, or reversing direction, was 9.3 ± 0.5 μm and the maximum distance was ~70 μm (Fig. 5*D*). Importantly, these speeds and distances are characteristic for trafficking along microtubules (22–26). The polarity of the vesicular traffic was assessed by comparing the total traveled distances in each direction in the different kymographs (data not shown). Individual nanotubes sometimes, but not always, showed a small net transport of vesicles in one direction.

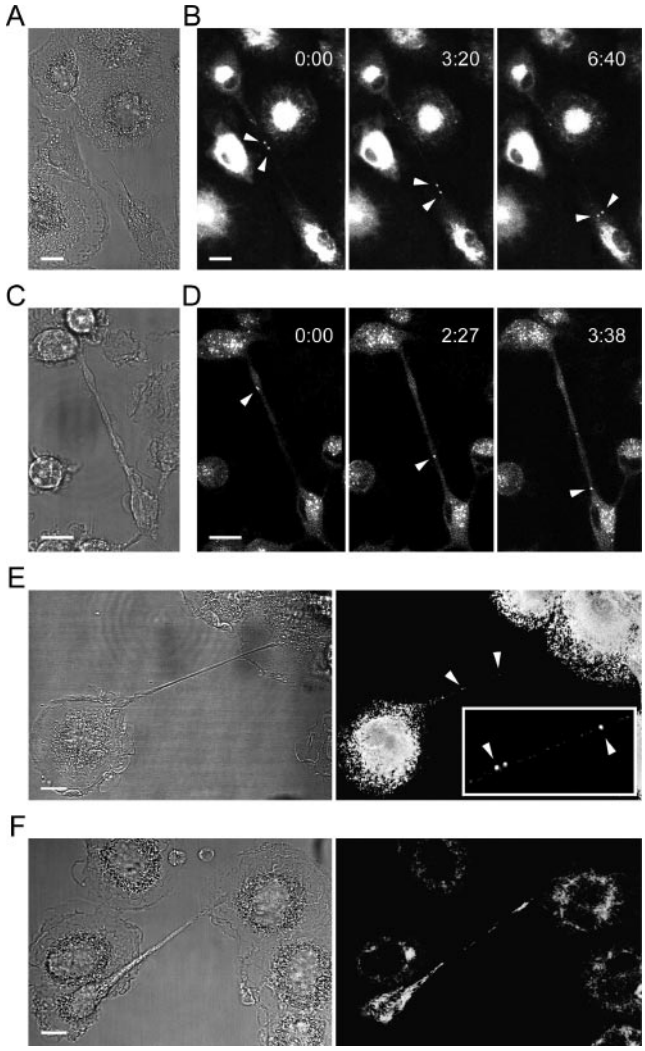

FIGURE 4. Endosomes, lysosomes, and mitochondria traffic within thick membrane nanotubes. *A*, Brightfield image of two macrophages connected by a thick membrane nanotube is shown. *B*, Time-lapse imaging shows several DiD-labeled vesicles (white) inside the membrane nanotube. Arrowheads mark two bright vesicles that moved along the nanotube and into the cytoplasm of one of the connected cells. *C–D*, Analogous data as in *A* and *B*, but cells were labeled with LysoTracker, which stained acidic lysosomes (white). *E* and *F*, Reconstructions from several optical slices. *E*, Punctuate staining of LAMP-1 in a thick membrane nanotube connecting two macrophages. Expanded section of the tube (*inset*) shows three bright vesicles (arrowheads). *F*, Two macrophages connected by a thick membrane nanotube containing mitochondria stained with MitoTracker (*right*; white). Time format is minutes:second. Scale bar, 20 μm.

ATP- and cytoskeletal-dependent processes are required for vesicular transport within membrane nanotubes

We next set out to probe the specific requirements for vesicular transport inside nanotubes by treating cells with drugs while being imaged. Kymographs were plotted before and after the addition of each drug to clearly reveal the movements of vesicles. Individual membrane nanotubes containing lipid vesicles, stained by DiD, were imaged before (Fig. 6*A*) and after (Fig. 6*B*) addition of 100

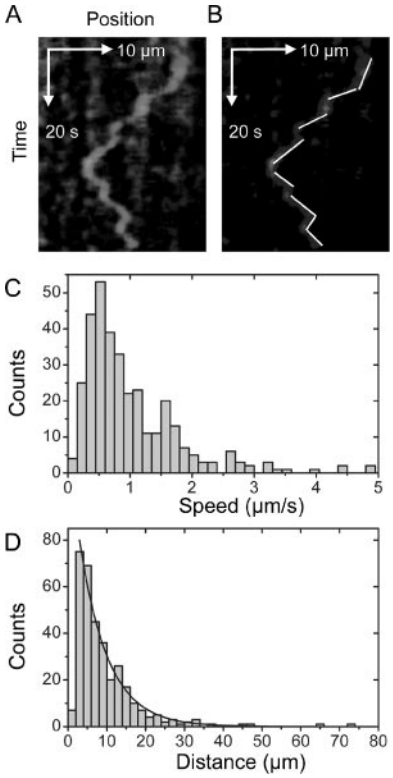

FIGURE 5. Vesicles move bidirectionally in a stepwise manner within thick membrane nanotubes. *A*, Kymograph from a section within a nanotube shows how the movement of vesicles could be followed and analyzed. The vesicle trajectory is visualized as the bright streaked white line. A sloped line corresponds to the vesicle moving and a vertical line corresponds to the vesicle being still. It is clearly seen that this vesicle moved in a stepwise and bidirectional manner. *B*, Quantification of vesicle speeds and distances traveled was done by using the coordinates of lines drawn within kymographs, as exemplified by the lines shown. A vesicle's "run" is defined as a period of continuous movement before a vesicle changes speed, transiently stops, or changes direction. *C*, Distribution of speeds and distances for individual vesicular runs ($n = 337$) measured over 10 kymographs depicting nanotubes connecting macrophages. The average speed was 1.01 ± 0.04 μm/s, maximum 4.9 μm/s, and the mean distance was 9.3 ± 0.5 μm, maximum 72 μm. *D*, The distribution in distances traveled (omitting distances <2 μm) has been fitted to an exponential decay with decay constant 7.3 μm (black line).

mM azide to the cell culture. Addition of azide abruptly abrogated vesicle movement, as evident by the appearance of vertical lines in the kymograph of a nanotube after the addition of azide (Fig. 6*B*). Thus, vesicular traffic within membrane nanotubes requires ATP-dependent processes.

To test whether specific cytoskeletal processes were involved in vesicular traffic within nanotubes, cells were incubated with the actin-depolymerizing drugs, latrunculin B or cytochalasin D, or the microtubule-destabilizing drugs, colchicine or nocodazole. Addition of 10 μM colchicine or 15 μM nocodazole stopped vesicle movement (Fig. 6, *C–F*). Nocodazole treatment sometimes caused gross changes to the morphology of the nanotubes before the effect on vesicular traffic could be assessed. Similar changes to the morphology of nanotubes were found when 10 μM cytochalasin D or 0.3–10 μM latrunculin B was added (supplemental videos 9 and 10).[5] Thus, trafficking of vesicles within thick nanotubes requires microtubules, and cytoskeletal proteins are important for maintaining the integrity of both types of membrane nanotubes.

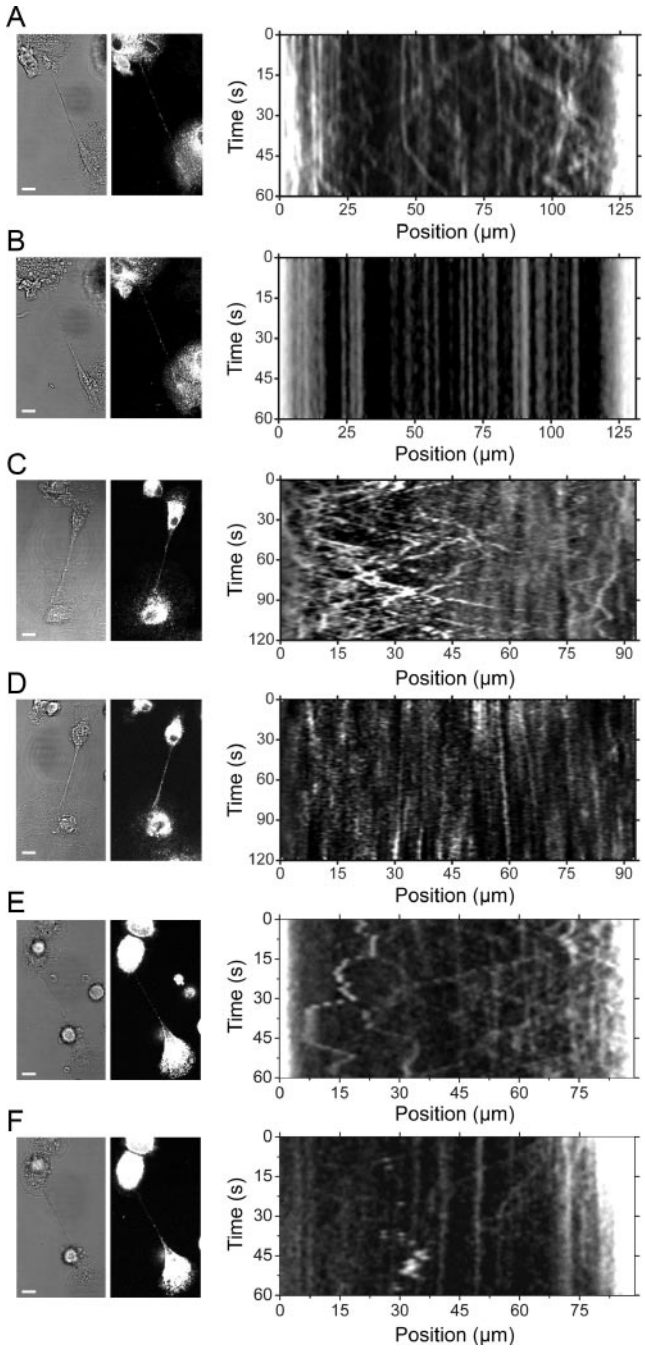

FIGURE 6. Vesicular transport along membrane nanotubes requires ATP- and microtubules. Membrane nanotubes between macrophages containing motile fluorescent lipid vesicles were imaged before and after the addition of drugs. *A*, Brightfield and fluorescence images of a membrane nanotube before treatment with azide are shown. The kymograph for the time-lapse sequence shows several streaked trajectories corresponding to motile vesicles within the nanotube. *B*, In contrast, after treatment with 100 mM azide vesicles stopped, resulting in vertical lines in the corresponding kymograph. *C–F*, Membrane nanotube before (*C* and *E*) and after (*D* and *F*) addition of the microtubule destabilizing agent colchicine (*C* and *D*) or nocodazole (*E* and *F*). Kymographs show that colchicine and nocodazole also abrogated vesicular transport. Scale bar, 20 μm.

ATP-dependent but not microtubule-dependent processes are required for surfing along thin membrane nanotubes

To test whether surface transport along membrane nanotubes also required ATP-dependent processes, streptavidin-coated beads

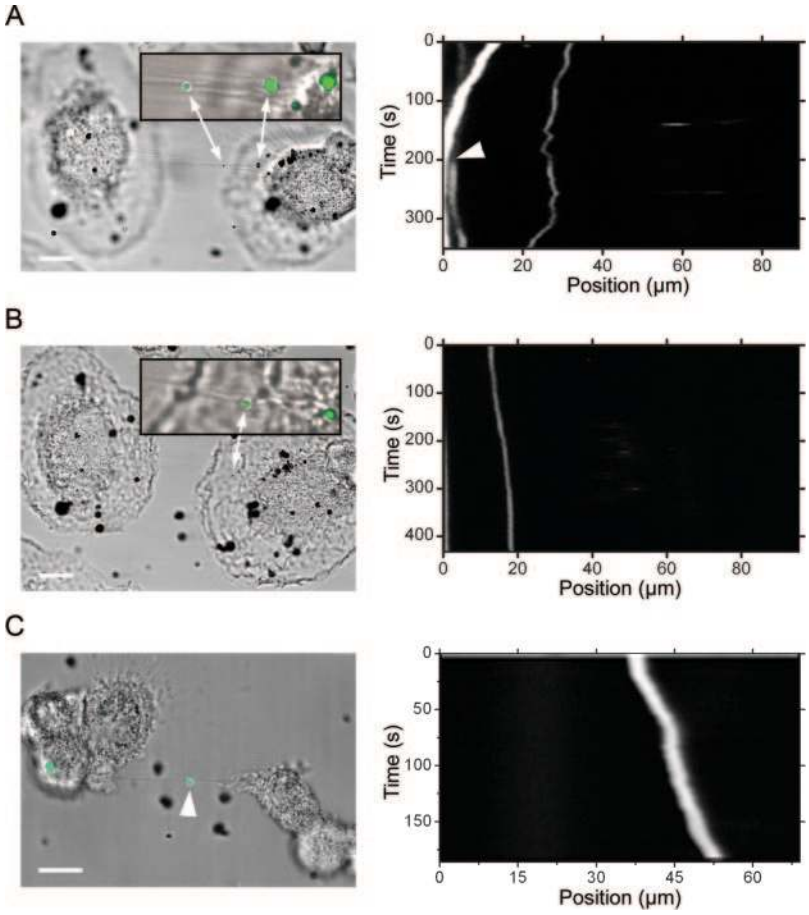

FIGURE 7. Surfing requires ATP but is independent of intact microtubules. *A*, Brightfield and corresponding kymograph showing two beads being transported along the surface of a thin nanotube before addition of azide. An enlarged view (*inset*) of the nanotube with the fluorescent beads bound to it (green). After ~200 s, one of the beads reached the connecting cell body (arrowhead in kymograph). *B*, After addition of azide, the bead that was still bound to the nanotube (*inset*) stopped moving, seen as a nearly vertical line in the kymograph ($n = 5$). *C*, Brightfield image and corresponding kymograph of a bead (arrowhead; green) bound to a nanotube in medium containing 10 μM colchicine ($n = 5$). Scale bar, 20 μm.

bound to thin nanotubes of surface-biotinylated macrophages were imaged before (Fig. 7*A*) and after (Fig. 7*B*) addition of azide. ATP depletion efficiently stopped beads surfing along nanotubes. In contrast to the vesicular transport, surfing of beads was unaffected by the addition of 10 μM colchicine (Fig. 7*C*). Abrogation of intracellular vesicular transport within the cell bodies confirmed that colchicine was effective in inhibiting microtubule-mediated traffic within these cells (data not shown). Thus, traffic of cargo bound to the surface of thin membrane nanotubes requires ATP-dependent processes but not microtubules.

Discussion

Recently, there has been much interest in immune cell membrane nanotubes, particularly because transmission of calcium fluxes between myeloid cells has been shown to occur via such nanotubes (13, 19, 27–29). This area of research is still in its infancy and finding out the possible mechanisms by which nanotubes can mediate communication between cells is central. For this it is important to know the cytoskeletal composition of membrane nanotubes and whether all membrane nanotubes are alike. We report here that there is a surprising heterogeneity in the structure of membrane nanotubes connecting human monocyte-derived macrophages. Specifically, thicker nanotubes contained both F-actin and microtubules, whereas thinner nanotubes contained only F-actin. Importantly, we demonstrated that these distinct nanotubular structures support specific mechanisms for distal interactions between cells. Nanotubes containing microtubules traffic vesicles over long distances, while bacteria "surf" along nanotubes lacking microtubules using a constitutive flow of the nanotube surface.

Surface transport along thin nanotubes was found to be dependent on ATP but independent of microtubules because colchicine has no effect on surface transport and these connections were not accessed by EB1-GFP nor stained by mAb against α-tubulin. Instead, it is likely that surfing of bacteria and beads on nanotubes uses mechanisms analogous to recent observations of surfing of viral particles along filopodia (15) and the retrograde flow observed in filopodia and retraction fibers (30–32). Concurrent with transport of beads and bacteria along the surface of thin nanotubes, brightfield images revealed "particles" that traffic along thin nanotubes with a speed of 0.10 ± 0.01 μm/s and integrated with the cell body as they reached the base of the tubular connection (data not shown). This is reminiscent of "nodules" previously observed to travel in retraction fibers connecting epithelial cells to the substratum (30, 32). The nodules observed by Cramer and Mitchison (30) were rich in actin and traveled monotonously toward the cell body along stationary actin filaments with speeds of around 0.04–0.09 μm/s. Thus, in addition to the surface flow there may also be mechanisms that support transport of molecules or organelles within thin membrane nanotubes.

Transport of vesicles, including late endosomes and lysosomes, however, were only observed inside thicker nanotubes connecting macrophages. Vesicles moved in a stepwise manner, with speeds and distances consistent with previous quantitative measurements of microtubule-based vesicular traffic (22–26). Moreover, their movement was specifically abrogated by the microtubule destabilizing drugs, colchicine and nocodazole, as well as azide. Thus, the presence of microtubules, only found in thicker nanotubes, is essential for vesicular traffic. Vesicles were observed to traverse the full length of nanotubes, i.e., many tens of microns, from the connection with one cell body all the way into the cytoplasm of the other connected cell. It is therefore possible that, for example, cross-presentation could be facilitated by the intercellular transfer

of Ag or MHC class II-rich vesicles (33) via membrane nanotubes. Vesicles could directly transfer from within nanotubes into the connecting cell body (1) or alternatively could deliver their contents across a small synaptic contact between a nanotube and cell body.

In addition to endosomes and lysosomes, we also found that mitochondria can access thick nanotubes. It has recently been shown that aerobic respiration of cells with dysfunctional mitochondria can be rescued by transfer of whole mitochondria or mitochondria DNA from other, undamaged cells (34). Thus, one mechanism by which the reported exchange of mitochondria could occur is via membrane nanotubes.

It is currently unknown to what extent nanotubes exist, and whether they have any function in vivo. However, cells in the imaginal disc of *Drosophila* can form long actin-rich protrusions called cytonemes, believed to be important for signaling transduction between cells (35, 36). Studies using two-photon microscopy have demonstrated that it is perhaps technically feasible to detect membrane tethers between immune cells in lymph nodes (37). Thus a major next goal must to be attempt detection of membrane nanotubes in vivo, as recently achieved for the visualizing the prototypical bulls-eye arrangement of proteins at a T cell immune synapse (38). Broadly, it is possible that communication mediated by long-range physical connections among immune cells is more widespread than previously thought. This report demonstrates that structurally distinct membrane nanotubes between macrophages can support different types of intercellular traffic. Thus, macrophages may use membrane nanotubes to interact over long distances with far more complexity and specificity compared with using soluble secretions alone.

Acknowledgments

We thank members of our laboratory for useful discussions, and Douglas Young, Imperial College (London, U.K.), for providing *Mycobacterium bovis* BCG-GFP.

Disclosures

The authors have no financial conflict of interest.

References

1. Rustom, A., R. Saffrich, I. Markovic, P. Walther, and H.-H. Gerdes. 2004. Nanotubular highways for intercellular organelle transport. *Science* 303: 1007–1010.
2. Stinchcombe, J. C., G. Bossi, S. Booth, and G. M. Griffiths. 2001. The immunological synapse of CTL contains a secretory domain and membrane bridges. *Immunity* 15: 751–761.
3. Önfelt, B., S. Nedvetzki, K. Yanagi, and D. M. Davis. 2004. Cutting edge: Membrane nanotubes connect immune cells. *J. Immunol.* 173: 1511–1513.
4. Arnold, P. Y., D. K. Davidian, and M. D. Mannie. 1997. Antigen presentation by T cells: T cell receptor ligation promotes antigen acquisition from professional antigen-presenting cells. *Eur. J. Immunol.* 27: 3198–3205.
5. Huang, J. F., Y. Yang, H. Sepulveda, W. Shi, I. Hwang, P. A. Peterson, M. R. Jackson, J. Sprent, and Z. Cai. 1999. TCR-Mediated internalization of peptide-MHC complexes acquired by T cells. *Science* 286: 952–954.
6. Vanherberghen, B., K. Andersson, L. M. Carlin, E. N. Nolte-'t Hoen, G. S. Williams, P. Höglund, and D. M. Davis. 2004. Human and murine inhibitory natural killer cell receptors transfer from natural killer cells to target cells. *Proc. Natl. Acad. Sci. USA* 101: 16873–16878.
7. Carlin, L. M., K. Eleme, F. E. McCann, and D. M. Davis. 2001. Intercellular transfer and supramolecular organization of human leukocyte antigen C at inhibitory natural killer cell immune synapses. *J. Exp. Med.* 194: 1507–1517.
8. Sjöström, A., M. Eriksson, C. Cerboni, M. H. Johansson, C. L. Sentman, K. Kärre, and P. Höglund. 2001. Acquisition of external major histocompatibility complex class I molecules by natural killer cells expressing inhibitory Ly49 receptors. *J. Exp. Med.* 194: 1519–1530.
9. Hudrisier, D., and P. Bongrand. 2002. Intercellular transfer of antigen-presenting cell determinants onto T cells: molecular mechanisms and biological significance. *FASEB J.* 16: 477–486.
10. Joly, E., and D. Hudrisier. 2003. What is trogocytosis and what is its purpose? *Nat. Immunol.* 4: 815.
11. Puaux, A. L., J. Campanaud, A. Salles, X. Preville, B. Timmerman, E. Joly, and D. Hudrisier. 2006. A very rapid and simple assay based on trogocytosis to detect and measure specific T and B cell reactivity by flow cytometry. *Eur. J. Immunol.* 36: 779–788.
12. Zimmer, J., V. Ioannidis, and W. Held. 2001. H-2D ligand expression by $Ly49A^+$ natural killer (NK) cells precludes ligand uptake from environmental cells: implications for NK cell function. *J. Exp. Med.* 194: 1531–1539.
13. Watkins, S. C., and R. D. Salter. 2005. Functional connectivity between immune cells mediated by tunneling nanotubules. *Immunity* 23: 309–318.
14. Salter, R. D., R. J. Tuma-Warrino, P. Q. Hu, and S. C. Watkins. 2004. Rapid and extensive membrane reorganization by dendritic cells following exposure to bacteria revealed by high-resolution imaging. *J. Leukocyte Biol.* 75: 240–243.
15. Lehmann, M. J., N. M. Sherer, C. B. Marks, M. Pypaert, and W. Mothes. 2005. Actin- and myosin-driven movement of viruses along filopodia precedes their entry into cells. *J. Cell Biol.* 170: 317–325.
16. Davies, J. Q., and S. Gordon. 2005. Isolation and culture of human macrophages. *Methods Mol. Biol.* 290: 105–116.
17. Humphreys, I. R., G. R. Stewart, D. J. Turner, J. Patel, D. Karamanou, R. J. Snelgrove, and D. B. Young. 2006. A role for dendritic cells in the dissemination of mycobacterial infection. *Microbes Infect.* 8: 1339–1346.
18. Mimori-Kiyosue, Y., N. Shiina, and S. Tsukita. 2000. The dynamic behavior of the APC-binding protein EB1 on the distal ends of microtubules. *Curr. Biol.* 10: 865–868.
19. Önfelt, B., M. A. Purbhoo, S. Nedvetzki, S. Sowinski, and D. M. Davis. 2005. Long-distance calls between cells connected by tunneling nanotubules. *Sci. STKE* 313: pe55.
20. Gatfield, J., and J. Pieters. 2000. Essential role for cholesterol in entry of mycobacteria into macrophages. *Science* 288: 1647–1650.
21. Tailleux, L., N. Pham-Thi, A. Bergeron-Lafaurie, J.-L. Herrmann, P. Charles, O. Schwartz, P. Scheinmann, P. H. Lagrange, J. de Blic, A. Tazi, et al. 2005. DC-SIGN induction in alveolar macrophages defines privileged target host cells for mycobacteria in patients with tuberculosis. *PLoS Med.* 2: e381.
22. Kural, C., H. Kim, S. Syed, G. Goshima, V. I. Gelfand, and P. R. Selvin. 2005. Kinesin and dynein move a peroxisome in vivo: a tug-of-war or coordinated movement? *Science* 308: 1469–1472.
23. King, S. J., and T. A. Schroer. 2000. Dynactin increases the processivity of the cytoplasmic dynein motor. *Nat. Cell Biol.* 2: 20–24.
24. Nishiura, M., T. Kon, K. Shiroguchi, R. Ohkura, T. Shima, Y. Y. Toyoshima, and K. Sutoh. 2004. A single-headed recombinant fragment of *Dictyostelium* cytoplasmic dynein can drive the robust sliding of microtubules. *J. Biol. Chem.* 279: 22799–22802.
25. Smith, G. A., L. Pomeranz, S. P. Gross, and L. W. Enquist. 2004. Local modulation of plus-end transport targets herpesvirus entry and egress in sensory axons. *Proc. Natl. Acad. Sci. USA* 101: 16034–16039.
26. Gross, S. P. 2004. Hither and yon: a review of bi-directional microtubule-based transport. *Phys. Biol.* 1: R1–R11.
27. Baluška, F., A. Hlavacka, D. Volkmann, and D. Menzel. 2004. Getting connected: actin-based cell-to-cell channels in plants and animals. *Trends Cell Biol.* 14: 404–408.
28. Baluška, F., D. Volkmann, and P. W. Barlow. 2004. Cell bodies in a cage. *Nature* 428: 371.
29. Roda-Navarro, P., M. Vales-Gomez, S. E. Chisholm, and H. T. Reyburn. 2006. Transfer of NKG2D and MICB at the cytotoxic NK cell immune synapse correlates with a reduction in NK cell cytotoxic function. *Proc. Natl. Acad. Sci. USA* 103: 11258–11263.
30. Cramer, L. P., and T. J. Mitchison. 1997. Investigation of the mechanism of retraction of the cell margin and rearward flow of nodules during mitotic cell rounding. *Mol. Biol. Cell* 8: 109–119.
31. Mallavarapu, A., and T. Mitchison. 1999. Regulated actin cytoskeleton assembly at filopodium tips controls their extension and retraction. *J. Cell Biol.* 146: 1097–1106.
32. Mitchison, T. J. 1992. Actin based motility on retraction fibers in mitotic PtK2 cells. *Cell Motil. Cytoskeleton* 22: 135–151.
33. Peters, P. J., G. Raposo, J. J. Neefjes, V. Oorschot, R. L. Leijendekker, H. J. Geuze, and H. L. Ploegh. 1995. Major histocompatibility complex class II compartments in human B lymphoblastoid cells are distinct from early endosomes. *J. Exp. Med.* 182: 325–334.
34. Spees, J. L., S. D. Olson, M. J. Whitney, and D. J. Prockop. 2006. Mitochondrial transfer between cells can rescue aerobic respiration. *Proc. Natl. Acad. Sci. USA* 103: 1283–1288.
35. Hsiung, F., F. A. Ramírez-Weber, D. D. Iwaki, and T. B. Kornberg. 2005. Dependence of *Drosophila* wing imaginal disc cytonemes on Decapentaplegic. *Nature* 437: 560–563.
36. Ramírez-Weber, F. A., and T. B. Kornberg. 1999. Cytonemes: cellular processes that project to the principal signaling center in *Drosophila* imaginal discs. *Cell* 97: 599–607.
37. Miller, M. J., O. Safrina, I. Parker, and M. D. Cahalan. 2004. Imaging the single cell dynamics of $CD4^+$ T cell activation by dendritic cells in lymph nodes. *J. Exp. Med.* 200: 847–856.
38. Barcia, C., C. E. Thomas, J. F. Curtin, G. D. King, K. Wawrowsky, M. Candolfi, W. D. Xiong, C. Liu, K. Kroeger, O. Boyer, et al. 2006. In vivo mature immunological synapses forming SMACs mediate clearance of virally infected astrocytes from the brain. *J. Exp. Med.* 203: 2095–2107.